22

Mathematical Morphology on Tensor Data Using the Loewner Ordering

Bernhard Burgeth, Martin Welk, Christian Feddern, and Joachim Weickert

Mathematical Image Analysis Group, Faculty of Mathematics and Computer Science, Saarland University, Building 27, 66041 Saarbrücken, Germany
{burgeth,welk,feddern,weickert}@mia.uni-saarland.de

Summary. The notions of maximum and minimum are the key to the powerful tools of greyscale morphology. Unfortunately these notions do not carry over directly to tensor-valued data. Based upon the Loewner ordering for symmetric matrices this chapter extends the maximum and minimum operation to the tensor-valued setting. This provides the ground to establish matrix-valued analogues of the basic morphological operations ranging from erosion/dilation to top hats. In contrast to former attempts to develop a morphological machinery for matrices, the novel definitions of maximal/minimal matrices depend continuously on the input data, a property crucial for the construction of morphological derivatives such as the Beucher gradient or a morphological Laplacian. These definitions are rotationally invariant and preserve positive semidefiniteness of matrix fields as they are encountered in DT-MRI data. The morphological operations resulting from a component-wise maximum/minimum of the matrix channels disregarding their strong correlation fail to be rotational invariant. Experiments on DT-MRI images as well as on indefinite matrix data illustrate the properties and performance of our morphological operators.

Key words: mathematical morphology, dilation, erosion, matrix-valued images, positive definite matrix, indefinite matrix, diffusion tensor MRI

22.1 Introduction

Since the late sixties mathematical morphology has proven itself a very valuable source of techniques and methods to process images: The path-breaking work of Matheron and Serra [12, 13] started a fruitful and extensive development of morphological operators and filters. Morphological tools have been established to perform noise suppression, edge detection, shape analysis, and skeletonisation for applications ranging from medical imaging to geological sciences, as it is documented in monographs [8, 14, 15, 16] and conference proceedings [6, 17]. It would be desireable to have the tools of morphology at our disposal to process tensor-valued images since nowadays the notion of image encompasses this data type as well. The variety of appearances of tensor

fields clearly calls for the development of appropriate tools for the analysis of such data structures because, just as in the scalar case, one has to remove noise and to detect edges and shapes by appropriate filters.

Median filtering [21], Chap. 21 by Welk et al., active contour models and mean curvature motion [4], Chap. 25 by Weickert et al., nonlinear regularisation methods and related diffusion filters [2, 18, 20], Chap. 22 by Suarez-Santana et al., Chap. 23 by Westin et al., Chap. 25 by Weickert et al., also Chap. 19 by Weickert and Welk, exist for matrix-valued data that genuinely exploit the interaction of the different matrix-channels.

First successful steps to extend morphological operations to matrix-valued data sets have been made in [3] where the basic operations dilation and erosion as well as opening and closing are transfered to the matrix-valued setting. However, the proposed approaches lack the continuous dependence on the input matrices. This makes the meaningful construction of morphological derivatives impossible.

The goal of this chapter is to present an alternative approach to morphological operators for tensor-valued images based on the Loewner ordering. This offers a greater potential for extensions and brings expedient notions of morphological derivatives within our reach. The morphological operations to be defined should work on the set $\mathrm{Sym}(n)$ of real symmetric $n \times n$ matrices and have to satisfy conditions such as:

i) Continuous dependence of the basic morphological operations on the matrices used as input for the aforementioned reasons.
ii) Rotational invariance.
iii) Preservation of the positive semidefiniteness of the matrix field since DT-MRI data sets, for instance, posses this property, see e.g. Chap. 5 by Alexander, Chap. 7 by Vilanova et al., Chap. 17 by Moakher and Batchelor.

Remarkably, the requirement of rotational invariance rules out the straightforward component-wise approach, as is shown in [3]. In this chapter we will introduce a novel notion of the minimum/maximum of a finite set of symmetric, not necessarily positive definite matrices. These notions will exhibit the above mentioned properties.

The chapter is structured as follows: The next section is devoted to a brief review of the greyscale morphological operations we aim to extend to the matrix-valued setting, starting from the basic erosion/dilation and reaching to the morphological equivalents of gradient and Laplacian. In Sect. 3 we present the crucial maximum and minimum operations for matrix-valued data and investigate some of their relevant properties. We report the results of our experiments with various morphological operators applied to real DT-MRI images as well as indefinite tensor fields from fluid mechanics in Sect. 4. Section 5 offers concluding remarks.

22.2 Brief Review of Scalar Morphology

In grey scale morphology an image is represented by a scalar function $f(x, y)$ with $(x, y) \in \mathbb{R}^2$. The so-called *structuring element* is a set B in $\mathbb{R}^2$ determining the neighbourhood relation of pixels. In this chapter we restrict ourselves to flat greyscale morphology where this binary type of structuring element is used. Then greyscale *dilation* $\oplus$, resp., *erosion* $\ominus$ replaces the greyvalue of the image $f(x, y)$ by its supremum, resp., infimum within the mask B:

$$\begin{aligned}(f \oplus B)(x, y) &:= \sup\{f(x-x', y-y') \mid (x', y') \in B\}\,,\\ (f \ominus B)(x, y) &:= \inf\{f(x+x', y+y') \mid (x', y') \in B\}\,.\end{aligned}$$

By concatenation other operators are constructed such as *opening* and *closing*,

$$f \circ B := (f \ominus B) \oplus B\,, \qquad f \bullet B := (f \oplus B) \ominus B\ ,$$

the *white top-hat* and its dual, the *black top-hat*

$$\mathrm{WTH}(f) := f - (f \circ B)\,, \qquad \mathrm{BTH}(f) := (f \bullet B) - f\,,$$

finally, the *self-dual top-hat*,

$$\mathrm{SDTH}(f) := (f \bullet B) - (f \circ B)\ .$$

In an image the boundaries or edges of objects are the loci of high greyvalue variations and those can be detected by gradient operators. Erosion and dilation are also the elementary building blocks of the basic morphological gradients. The so-called *Beucher gradient*

$$\varrho_B(f) := (f \oplus B) - (f \ominus B)$$

is an analog to the norm of the gradient $\|\nabla f\|$ if an image is considered as a differentiable function. Other useful approximations to $\|\nabla f\|$ are the *internal* and *external gradient*,

$$\varrho_B^-(f) := f - (f \ominus B)\,, \qquad \varrho_B^+(f) := (f \oplus B) - f\,.$$

We also present a morphological equivalent for the Laplace operator $\Delta f = \partial_{xx} f + \partial_{yy} f$ suitable for matrix-valued data. The *morphological Laplacian* has been introduced in [19]. We consider a variant given by the difference between external and internal gradient:

$$\Delta_m f := \varrho_B^+(f) - \varrho_B^-(f) = (f \oplus B) - 2 \cdot f + (f \ominus B)\ .$$

This form of a Laplacian represents the second derivative $\partial_{\eta\eta} f$ where η denotes the direction of the steepest slope. $\Delta_m f$ is matrix-valued, but $\mathrm{trace}(\Delta_m f)$ provides us with useful information: Regions where $\mathrm{trace}(\Delta_m f) \leq 0$ can be viewed as the influence zones of maxima while those areas with

$\mathrm{trace}(\Delta_m f) \geq 0$ are influence zones of minima. It therefore allows us to distinguish between influence zones of minima and maxima in the image f. This is crucial for the design of so-called *shock filters*.

The basic idea underlying shock filtering is applying either a dilation or an erosion to an image, depending on whether the pixel is located within the influence zone of a minimum or a maximum [10]:

$$\delta_B(f) := \begin{cases} f \oplus B & \text{if} \quad \mathrm{trace}(\Delta_m f) \leq 0\,, \\ f \ominus B & \text{else}\,. \end{cases} \tag{22.1}$$

The shock filter expands local minima and maxima at the cost of regions with intermediate greyvalues. When iterated experimental results in greyscale morphology suggest that a non-trivial steady state exists characterised by a piecewise constant segmentation of the image.

In the scalar case the zero-crossings $\Delta f = 0$ can be interpreted as edge locations [7, 9, 11]. We will also use the trace of the morphological Laplacian in this manner to derive an edge map.

22.3 Extremal Matrices in the Loewner Ordering

There is a natural partial ordering on $\mathrm{Sym}(n)$, the so-called *Loewner ordering* defined via the cone of positive semidefinite matrices $\mathrm{Sym}^+(n)$ by

$$A, B \in \mathrm{Sym}(n): \quad A \geq B :\Leftrightarrow A - B \in \mathrm{Sym}^+(n)\,,$$

i.e. if and only if $A - B$ is positive semidefinite.

This partial ordering is *not* a lattice ordering, that is, the notion of a unique supremum and infimum with respect to this ordering does not exist [1]. Nevertheless, given any finite set of symmetric matrices $\mathcal{A} = \{A_1, \ldots, A_n\}$, we will be able to identify suitable maximal, resp., minimal matrices

$$\overline{A} := \max \mathcal{A} \quad \text{resp.}, \quad \underline{A} := \min \mathcal{A}\,.$$

For presentational reasons we restrict ourselves from now on to the case of 2×2-matrices in $\mathrm{Sym}(2)$. The 3×3-case is treated similarly but is technically more involved.

To find these extremal matrices for a set $\mathcal{A}$ we proceed as follows: The cone $\mathrm{Sym}^+(2)$ can be visualized in 3D using the bijection

$$\begin{pmatrix} \alpha & \beta \\ \beta & \gamma \end{pmatrix} \longleftrightarrow \frac{1}{\sqrt{2}} \begin{pmatrix} 2\beta \\ \gamma - \alpha \\ \gamma + \alpha \end{pmatrix}, \text{ resp., } \frac{1}{\sqrt{2}} \begin{pmatrix} z - y & x \\ x & z + y \end{pmatrix} \longleftrightarrow \begin{pmatrix} x \\ y \\ z \end{pmatrix}.$$

This mapping creates an isometrically isomorphic image of the cone $\mathrm{Sym}^+(2)$ in the Euclidean space $\mathbb{R}^3$ given by $\{(x, y, z)^\top \in \mathbb{R}^3 | \sqrt{x^2 + y^2} \leq z\}$ and

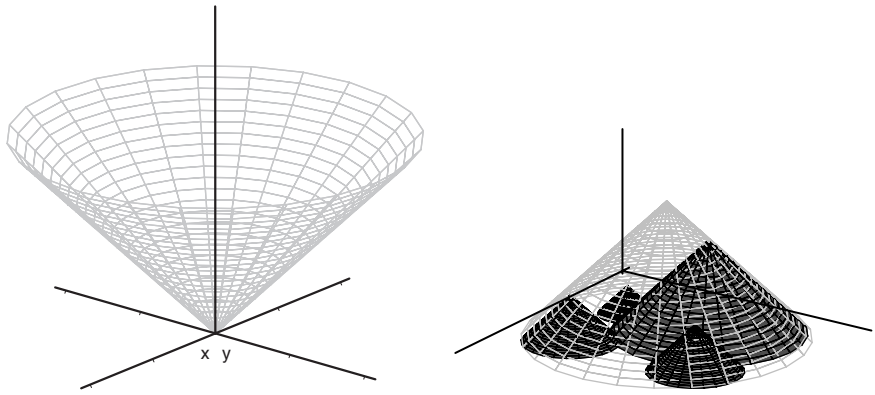

Fig. 22.1. (**a**) *Left*: Image of the Loewner cone $\mathrm{Sym}^+(2)$. (**b**) *Right*: Cone covering four penumbras of other matrices. The tip of each cone represents a symmetric 2×2 matrix in $\mathbb{R}^3$. For each cone the radius and the height are equal

depicted in Fig. 22.1(a). For $A \in \mathrm{Sym}(2)$ the set $P(A) = \{Z \in \mathrm{Sym}(2) | A \geq Z\}$ denotes the penumbra of the matrix A. It corresponds to a cone with vertex in A and a circular base in the x-y-plane:

$$P(A) \cap \{z = 0\} = \text{ circle with centre } \left(\sqrt{2}\beta, \frac{\gamma - \alpha}{\sqrt{2}}\right) \text{ and radius } \frac{\mathrm{trace}(A)}{\sqrt{2}} \,.$$

Considering the associated penumbras of the matrices in $\mathcal{A}$ the search for the *maximal matrix* $\overline{A}$ amounts to determine the smallest cone covering all the penumbras of $\mathcal{A}$; see Fig. 22.1(b). Note that the height of a penumbra in the x-y-plane is equal to the radius of its base, namely $\frac{\mathrm{trace}(A)}{\sqrt{2}}$. Hence a penumbra is already uniquely determined by the circle constituting its base. This implies that the search for a maximal matrix comes down to find the smallest circle enclosing the base-circles of the matrices in $\mathcal{A}$. This is a non-trivial problem in computer graphics. An efficient numerical solution for finding the smallest ball enclosing a given number of points has been implemented in C++ only recently by Gärtner [5].

By sampling the basis circles we use this implementation for the calculation of the smallest circle enclosing them. This gives us the smallest covering cone and hence the maximal matrix $\overline{A}$. A suitable *minimal matrix* $\underline{A}$ is obtained via the formula

$$\underline{A} = \left(\max(A_1^{-1}, \ldots, A_n^{-1})\right)^{-1}$$

inspired by the well-known relation $\min(a_1, \ldots, a_n) = \left(\max(a_1^{-1}, \ldots, a_n^{-1})\right)^{-1}$ valid for real numbers $a_1, \ldots, a_n$. Furthermore, inversion preserves positive definiteness as well as rotational invariance. For $i = 1, \ldots, n$ we have $\underline{A} \leq A_i \leq \overline{A}$ with respect to the Loewner ordering. We emphasise that $\overline{A}$ and $\underline{A}$ depend continuously on $A_1, \ldots, A_n$ by their construction. Also the

rotational invariance is preserved, since the Loewner ordering is already rotational invariant: $A \geq B \iff UAU^\top \geq UBU^\top$ holds for any orthogonal matrix U. Finally it is important to note that if all the A_i are positive definite then so is $\overline{A}$ as well as $\underline{A}$.

Nevertheless, the definitions of the matrices $\overline{A}$ and $\underline{A}$ are still meaningful for matrices that are not positive definite as long as they have a nonnegative trace (since it corresponds to a radius in the construction above). It also becomes evident from their construction that in general neither $\overline{A}$ nor $\underline{A}$ coincide with any of the A_i: $\overline{A}, \underline{A} \notin \mathcal{A}$.

With these essential notions of suitable maximal and minimal matrices $\overline{A}$ and $\underline{A}$ at our disposal the definitions of the higher morphological operators carry over essentially verbatim, with one exception:

The morphological Laplacian Δ_m as defined in Sect. 2 is a matrix. In equation (22.1) we used the *trace* of the morphological Laplacian to steer the interwoven dilation-erosion process, and to create an edge map.

A word of care has to be stated: unlike in the scalar-valued setting the minimum/maximum are not associative, e.g. $\max(A_1, A_2, A_3)$ generally can not be obtained by evaluating $\max(\max(A_1, A_2), A_3)$. This entails a loss of the semi-group property of the derived dilation and erosion. Clearly this has no effects as long as these morphological operations are not iterated.

In the next section we will apply various morphological operators to positive definite DT-MRI images as well as to indefinite matrix fields representing a flow field.

22.4 Experimental Results

In our numerical experiments we use two data sets:

1) Positive definite data. A 128×128 field of 2-D tensors which has been extracted from a 3-D DT-MRI data set of a human head. Those data are represented as ellipses via the level sets of the quadratic form $\{x^\top A^{-2} x | x \in \mathbb{R}^2\}$ associated with a matrix $A \in \mathrm{Sym}(n)$. The exponent -2 takes care of the fact that the small, resp., big eigenvalue corresponds to the semi-minor, resp., semi-major axis of the ellipse. The color coding of the ellipses reflects the direction of their principle axes. Another technical issue is that our DT-MRI data set of a human head contains not only positive definite matrices. Because of the quantisation there are singular matrices (particularly, a lot of zero matrices outside the head segment) and even matrices with negative eigenvalues. The negative values are of very small absolute value, and they result from measurement imprecision and quantisation errors. While such values do not constitute a problem in the dilation process, the erosion, relying on inverses of positive definite matrices, has to be regularised. Instead of the exact inverse A^{-1} of a given matrix A we use therefore $(A + \varepsilon I)^{-1}$ with a small positive ε.

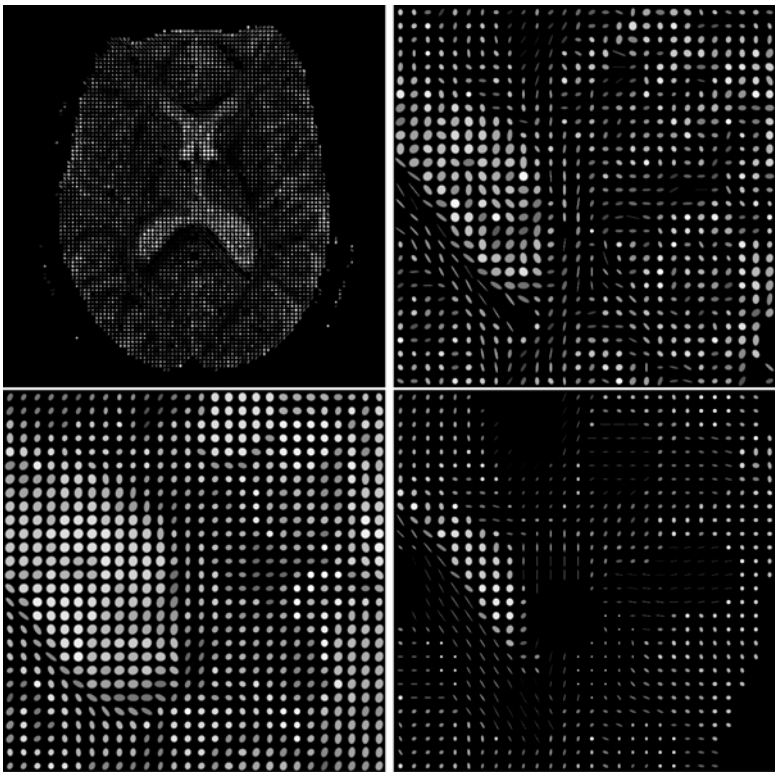

Fig. 22.2. (**a**) *Top left*: 2-D tensor field extracted from a DT-MRI data set of a human head. (**b**) *Top right*: enlarged section of left image. (**c**) *Bottom left*: dilation with DSE($\sqrt{5}$). (**d**) *Bottom right*: erosion with DSE($\sqrt{5}$)

2) Indefinite data. An image of size 248×202 containing indefinite matrices and depicting a rate-of-deformation tensor field from a experiment in fluid dynamics. Here tensor-valued data are represented in the figures by greyvalue images which are subdivided in four tiles. Each tile corresponds to one matrix entry. A middle grey value represents the zero value; *Magnitude* information of the matrix-valued signals is essentially encoded in the trace of the matrix and thus in the main diagonal. Instead, the off-diagonal of a symmetric matrix encode anisotropy.

Figure 22.2 displays the original head image and an enlarged section of it as well as the effect of dilation and erosion with a disk-shaped structuring element of radius $\sqrt{5}$. For the sake of brevity we denote in the sequel this element by DSE($\sqrt{5}$). We encounter the expected enhancement or suppression of features in the image. As known from scalar-valued morphology, the shape of details in the dilated and eroded images mirrors the shape of the structuring element.

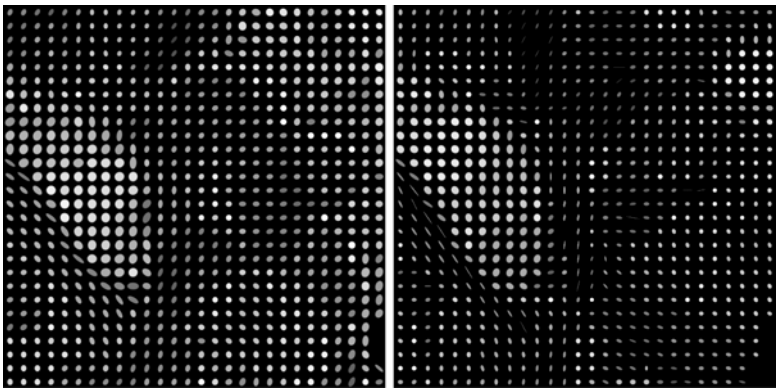

Fig. 22.3. (**a**) *Left*: closing with DSE($\sqrt{5}$). (**b**) *Right*: opening with DSE($\sqrt{5}$)

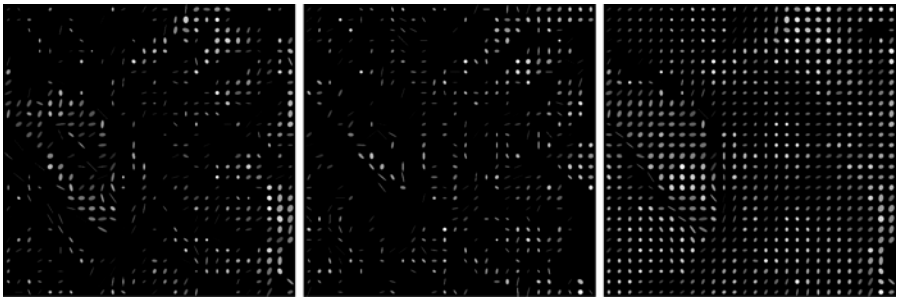

Fig. 22.4. (**a**) *Left*: white top hat with DSE($\sqrt{5}$). (**b**) *Middle*: black top hat with DSE($\sqrt{5}$). (**c**) *Right*: self-dual top hat with DSE($\sqrt{5}$)

In Figs. 22.3 and 22.7, the results of opening and closing operations are shown. In good analogy to their scalar-valued counterparts, both operations restitute the coarse shape and size of structures. Smaller details are eliminated by the opening operation, while the closing operation magnifies them. It also seems that the isotropy of the matrices is increased under both operations.

The top hat filters can be seen in Fig. 22.4. As in the scalar-valued case, the white top hat is sensitive for small-scale details formed by matrices with large eigenvalues, while the black top hat responds with high values to small-scale details stemming from matrices with small eigenvalues. The self-dual top hat as the sum of white and black top hat results in homogeneously high matrices rather evenly distributed in the image.

Figures 22.5 and 22.8 depict the internal and external morphological gradients and their sum, the Beucher gradient for positive and negative definite matrix-fields. It is no surprise that these operators respond to the presence of edges, the one-sided gradients more so than the Beucher gradient whose inertance is known. The images depicting the flow field show clearly that changes in the values of the matrices are well detected.

Fig. 22.5. (**a**) *Left*: external gradient with DSE($\sqrt{5}$). (**b**) *Middle*: internal gradient with DSE($\sqrt{5}$). (**c**) *Right*: Beucher gradient with DSE($\sqrt{5}$)

Fig. 22.6. (**a**) *Left*: morphological Laplacian with DSE($\sqrt{5}$). (**b**) *Middle*: result of shock filtering with DSE($\sqrt{5}$). (**c**) *Right*: edge map derived from zero crossings of the morphological Laplacian with DSE($\sqrt{5}$)

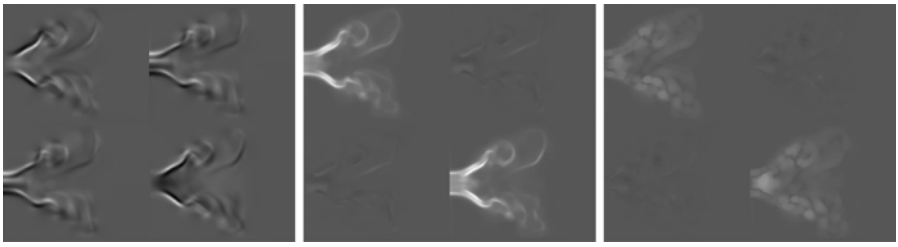

Fig. 22.7. (**a**) *Left*: original image of a flow field. (**b**) *Middle*: closing with DSE($\sqrt{5}$). (**c**) *Right*: opening with DSE($\sqrt{5}$)

The effect of the Laplacian Δ_{m} and its use for controlling a shock filter can be seen in Fig. 22.6: while applying dilation in pixels where the trace of the Laplacian is negative, it uses erosion wherever the trace of the Laplacian is positive. The result is an image in which regions with larger and smaller eigenvalues are sharper separated than in the original image. We also may concede some edge detection capabilities to the morphological Laplacian for tensor data. Image (c) in Fig. 22.6 displays an edge map derived by setting

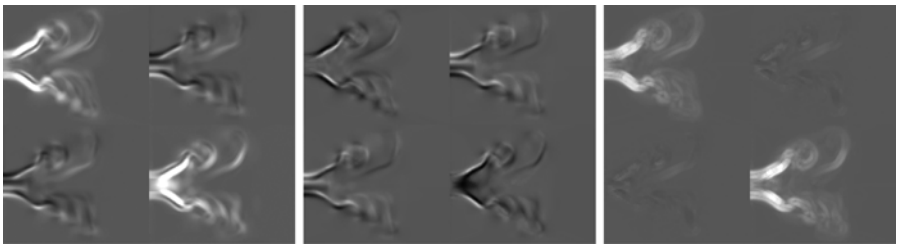

Fig. 22.8. (**a**) *Left*: external gradient with DSE($\sqrt{5}$). (**b**) *Middle*: internal gradient with DSE($\sqrt{5}$). (**c**) *Right*: Beucher gradient with DSE($\sqrt{5}$)

the pixel value to 255 if in that pixel the condition $-100 \leq \text{trace}(\Delta_m f) \leq 100$ is satisfied, and 0 if the absolute value of $\text{trace}(\Delta_m f)$ exceeds 100.

22.5 Conclusions

In this chapter we have extended fundamental concepts of mathematical morphology to the case of matrix-valued data. This has been achieved by determining maximal and minimal elements $\overline{A}$, $\underline{A}$ in the space of symmetric matrices $\text{Sym}(n)$ with respect to the Loewner ordering. These extremal elements serve as an suitable analogue for the continuous notion of maximum and minimum, which lie at the heart of mathematical morphology. As a consequence we were able not only to design the matrix-valued equivalents of basic morphological operations like dilation or erosion but also morphological derivatives and shock filters for tensor fields. In the experimental section the performance of the various morphological operations on positive definite as well as indefinite matrix-fields is documented.

Future work comprises the extension of the methodology to the demanding case of 3×3-matrix-fields as well a the development of more sophisticated morphological operators for matrix-valued data.

Acknowledgments

We are grateful to Anna Vilanova i Bartrolí (Eindhoven Institute of Technology) and Carola van Pul (Maxima Medical Center, Eindhoven) for providing us with the DT-MRI data set and for discussing questions concerning data conversion.

The fluid dynamics data set goes back to Wolfgang Kollmann (MAE Department, UC Davis) and has been kindly provided by Gerik Scheuermann (Institute for Computer Science, University of Leipzig). We would also like to thank Andrés Bruhn (Mathematical Image Analysis Group, Saarland University) for his valuable support in implementational issues.

References

1. J. M. Borwein and A. S. Lewis. *Convex Analysis and Nonlinear Optimization*. Springer, New York, 1999.
2. T. Brox, J. Weickert, B. Burgeth, and P. Mrázek. Nonlinear structure tensors. Technical report, Dept. of Mathematics, Saarland University, Saarbrücken, Germany, July 2004.
3. B. Burgeth, M. Welk, C. Feddern, and J. Weickert. Morphological operations on matrix-valued images. In T. Pajdla and J. Matas, editors, *Computer Vision – ECCV 2004, Part IV*, volume 3024 of *Lecture Notes in Computer Science*, pp. 155–167. Springer, Berlin, 2004.
4. C. Feddern, J. Weickert, B. Burgeth, and M. Welk. Curvature-driven PDE methods for matrix-valued images. *International Journal of Computer Vision*, 2005. In press.
5. B. Gärtner. http://www2.inf.ethz.ch/personal/gaertner/. WebPage last visited: July 2nd, 2004.
6. J. Goutsias, L. Vincent, and D. S. Bloomberg, editors. *Mathematical Morphology and its Applications to Image and Signal Processing*, volume 18 of *Computational Imaging and Vision*. Kluwer, Dordrecht, 2000.
7. R. M. Haralick. Digital step edges from zero crossing of second directional derivatives. *IEEE Transactions on Pattern Analysis and Machine Intelligence*, 6(1):58–68, 1984.
8. H. J. A. M. Heijmans. *Morphological Image Operators*. Academic Press, Boston, 1994.
9. R. Kimmel and A. M. Bruckstein. Regularized Laplacian zero crossings as optimal edge integrators. *International Journal of Computer Vision*, 53(3):225–243, 2003.
10. H. P. Kramer and J. B. Bruckner. Iterations of a non-linear transformation for enhancement of digital images. *Pattern Recognition*, 7:53–58, 1975.
11. D. Marr and E. Hildreth. Theory of edge detection. *Proceedings of the Royal Society of London, Series B*, 207:187–217, 1980.
12. G. Matheron. *Eléments pour une théorie des milieux poreux*. Masson, Paris, 1967.
13. J. Serra. *Echantillonnage et estimation des phénomènes de transition minier*. PhD thesis, University of Nancy, France, 1967.
14. J. Serra. *Image Analysis and Mathematical Morphology*, volume 1. Academic Press, London, 1982.
15. J. Serra. *Image Analysis and Mathematical Morphology*, volume 2. Academic Press, London, 1988.
16. P. Soille. *Morphological Image Analysis*. Springer, Berlin, 1999.
17. H. Talbot and R. Beare, editors. *Proc. Sixth International Symposium on Mathematical Morphology and its Applications*. Sydney, Australia, April 2002. http://www.cmis.csiro.au/ismm2002/proceedings/.
18. D. Tschumperlé and R. Deriche. Diffusion tensor regularization with constraints preservation. In *Proc. 2001 IEEE Computer Society Conference on Computer Vision and Pattern Recognition*, volume 1, pp. 948–953, Kauai, HI, December 2001. IEEE Computer Society Press.
19. L. J. van Vliet, I. T. Young, and A. L. D. Beckers. A nonlinear Laplace operator as edge detector in noisy images. *Computer Vision, Graphics and Image Processing*, 45(2):167–195, 1989.

20. J. Weickert and T. Brox. Diffusion and regularization of vector- and matrix-valued images. In M. Z. Nashed and O. Scherzer, editors, *Inverse Problems, Image Analysis, and Medical Imaging*, volume 313 of *Contemporary Mathematics*, pp. 251–268. AMS, Providence, 2002.
21. M. Welk, C. Feddern, B. Burgeth, and J. Weickert. Median filtering of tensor-valued images. In B. Michaelis and G. Krell, editors, *Pattern Recognition*, volume 2781 of *Lecture Notes in Computer Science*, pp. 17–24, Berlin, 2003. Springer.